Dynamics of High Energy Runaway Electrons in the Oak Ridge Tokamak

S. J. Zweben
H. Knoepfel

MASTER

OAK RIDGE NATIONAL LABORATORY

OPERATED BY UNION CARBIDE CORPORATION · FOR THE DEPARTMENT OF ENERGY

DISCLAIMER

This report was prepared as an account of work sponsored by an agency of the United States Government. Neither the United States Government nor any agency Thereof, nor any of their employees, makes any warranty, express or implied, or assumes any legal liability or responsibility for the accuracy, completeness, or usefulness of any information, apparatus, product, or process disclosed, or represents that its use would not infringe privately owned rights. Reference herein to any specific commercial product, process, or service by trade name, trademark, manufacturer, or otherwise does not necessarily constitute or imply its endorsement, recommendation, or favoring by the United States Government or any agency thereof. The views and opinions of authors expressed herein do not necessarily state or reflect those of the United States Government or any agency thereof.

DISCLAIMER

Portions of this document may be illegible in electronic image products. Images are produced from the best available original document.

ORNL/TM-6103

Contract No. W-7405-eng-26

FUSION ENERGY DIVISION

DYNAMICS OF HIGH ENERGY RUNAWAY ELECTRONS

IN THE OAK RIDGE TOKAMAK

S. J. Zweben

Oak Ridge Associated Universites
Graduate Participant

and

H. Knoepfel
On leave from Centro Gas Ionizzati
Frascati, Italy

Date Published – December 1977

NOTICE This document contains information of a preliminary nature. It is subject to revision or correction and therefore does not represent a final report.

DYNAMICS OF HIGH ENERGY RUNAWAY ELECTRONS

IN THE OAK RIDGE TOKAMAK

H. Knoepfel[*] and S. J. Zweben[†]

Oak Ridge National Laboratory
Oak Ridge, Tennessee 37830

ABSTRACT

Runaway electrons produced during normal discharges in the Oak Ridge Tokamak (ORMAK) have been studied with a hard x-ray diagnostic system along with most of the other diagnostics available on this machine. It is found that runaways can attain maximum energies of up to 10 MeV and be contained over times of typically 50 msec. A simple physical model is proposed that is consistent with most of the observed high energy runaway phenomena. Some properties of the overall runaway distribution generated in tokamaks are inferred from these results and are discussed in terms of runaway generation, acceleration, and transport.

I. INTRODUCTION

Runaway electrons keep appearing, under various discharge conditions, in most toroidal plasma devices.[1,2] This is not surprising, since the formation of runaway electrons is a fundamental physical effect that is intimately related to the conduction of current in an ionized gas.[3]

It is the purpose of this work to show, on the basis of some selected experimental results obtained during an extensive study of runaway phenomena in ORMAK,[4] that in some normal discharges:

1) An appreciable number of electrons can attain energies up to 10 MeV.

2) These runaways can be accelerated in the electric field of the discharge as (nearly) free electrons and are contained over times of typically 50 msec.

3) Most of the confinement effects can be ordered and understood in terms of a simple drift orbit model.

On the basis of these results, some properties of the overall runaway distribution generated in tokamaks are then inferred and discussed in terms of runaway generation, acceleration, and transport.

A practical consequence of these findings — pointing towards the use of these high energy runaways as a means to probe the plasma — is that whenever runaway electrons do not perform according to the drift orbit model, specific physical effects should exist in the discharge that alter their production rate, reduce their containment, or augment their friction in the plasma. Although some of these anomalous effects will be mentioned, in general this work is concerned with the runaway behavior in normal discharges in the absence of gross instability of the plasma or runaway components. In this case the high energy runaway behavior is generally consistent with the drift orbit model described in Sec. II.

The data reported in the following sections have been obtained from most of the standard diagnostic systems available on ORMAK; of particular relevance is the hard x-ray detection system that was developed for this study.[5] It is made up of two well collimated and shielded NaI (Tℓ*) scintillation detectors which look tangentially at the limiter and/or at other targets in the discharge chamber (Fig. 1); they allow a time- and space-resolved measurement of the bremsstrahlung energy and intensity spectrum. In addition, there are two other scintillation detectors and an ionization chamber located at various places around the machine to monitor the hard x-ray intensity. The scintillation data are stored and analyzed by hardware and software that are integrated into the ORMAK data analysis system.

II. DRIFT ORBIT MODEL

The experiments show that in ideal discharge conditions the high energy runaways behave basically as freely accelerated electrons. The trajectory of a free electron with kinetic energy $T = mc^2 (\gamma - 1)$ in a tokamak configuration consists of a fast gyration at the (toroidal, B_T) magnetic field Larmor frequency,

$$\Omega_T = \frac{eB_T}{\gamma m_o c} \quad , \tag{1}$$

about a guiding center whose path lies on a drift surface. This drift surface is the result of movement along the helical field lines and of the (vertical) drift with velocity

$$v_d = \frac{1}{R_o \Omega_T} \left(v_\parallel^2 + \frac{1}{2} v_\perp^2 \right) , \tag{2}$$

where R is the distance of the particle from the major axis. For runaway electrons ($v_\parallel \gg v_\perp$), the velocity is normally determined principally by the curvature drift, $v_d \simeq (v_\parallel)^2/(R\Omega_T)$. The projection of the helical movement onto a cross-sectional plane gives a circular movement with velocity $v_h = v_\parallel \frac{B_p}{B_T}$, where B_p is the poloidal field due to the plasma current. The combination of the v_d and v_h movements results in a projected trajectory that is approximately a circle shifted outward by the distance d_γ from the center of the current distribution (Fig. 1).

The conservation of canonical angular momentum,

$$P_\phi = \gamma m_o R v_\parallel - (e/c)\psi(r) , \tag{3}$$

in a steady-state condition can be used to calculate d_γ. For example, for a filamentary current (i.e., all current I flows within the runaway drift surface) the poloidal flux function is

$$\psi = \int_o^r B_p R dr = R_o(I/c)[1 + 2\ln(r/a)] . \tag{4}$$

Equating P_ϕ at point A (see Fig. 1, where $R \equiv R_o - r_c + d_\gamma$, $r \equiv r_c - d_\gamma$) and point B ($R \equiv R_o + r_c + d_\gamma$, $r \equiv r_c + d_\gamma$) gives finally

$$d_\gamma \simeq \frac{r_c^2}{2R_o} \frac{I_A}{I} , \tag{5}$$

where

$$I_A = \beta\gamma \frac{m_o c^2}{e} = 17 \sqrt{\gamma^2 - 1} \tag{6}$$

is the Alfvén current (in kiloamperes).

Other more realistic current profiles can be handled with the same method or can be determined numerically. For example, the insert of Fig. 2 shows some shifted orbits that just intersect the limiter in a typical ORMAK type B current profile,

$$j(r) = j_o[1 - (r/r_L)^3] \quad . \tag{7}$$

Experimentally, the runaway is detected through the bremsstrahlung produced when its orbit intersects the target (outer limiter) at a radius r_L. That occurs when $r_c + d_\gamma + d_p = r_L$, for example for a filamentary current profile when

$$\frac{I_A}{I} \simeq \frac{2R_o}{r_c}\left[\frac{r_L}{r_c} - 1 - \frac{d_p}{r_c}\right], \tag{8}$$

where d_p is the shift of the current distribution as measured by magnetic loops.[6] It can be shown[7] that for orbits with large radii the mean radius r_c at intersection (Fig. 1) is approximately identical with the radius of the magnetic surface on which the runaway started off before acceleration.

Equation (8) thus provides the relation between the unknown initial orbit radius r_c and the measurable kinetic energy of the electron when it finally hits the outer limiter. This intersection condition is plotted in Fig. 2, with similar curves relative to other current distributions.

This model may be extended to give further relations between measurable quantities and therefore to provide additional information on the runaway process. For example, the number of runaways ΔS_R driven into the limiter per unit time as a consequence of the orbit shift with d_p constant is given by

$$\frac{\Delta S_R}{\Delta t} = 4\pi^2 R \; r_c n_R \frac{\Delta d_\gamma}{\Delta t} \quad . \tag{9}$$

The velocity $\Delta d_\gamma/\Delta t$ with which the drift surfaces shift into the limiter can be calculated from Eq. (8) or Fig. 2 with the energy $[\gamma = \gamma(t)]$ and the current $[I = I(t)]$ both being measurable quantities. Since $S_R = S_R(t)$ can also be measured, it is thus possible to determine, within the

assumptions and precision of this method, the initial local runaway density $n_R = n_R(r_{ci})$.[8] However, with the limited precision of present experimental data, the results of such deductions are somewhat open to discussion.

The acceleration of runaway electrons can be described by considering an approximate model in which free electrons are accelerated from time t_o by the electric field E_ϕ along the toroidal direction ϕ ($v_\phi = v_{\parallel}$). The equation of motion is

$$\frac{d(\gamma m_o v_\phi)}{dt} = -eE_\phi$$

or

$$\frac{d \sqrt{\gamma^2 - 1}}{dt} = \frac{e}{m_o c} \frac{dA_\phi}{dt} \quad . \tag{10}$$

Here A_ϕ is the only component of the vector potential in this axisymmetric problem and is given by

$$A_\phi(r_R, t) = \int_{t_o}^{t} \frac{V_L(t)}{2\pi R_o} dt - F(r_R, t) \quad , \tag{11}$$

where V_L is the measurable loop voltage (along the toroidal discharge vessel) and $F(r_R, t)$ is an inductive correction term[9] that is roughly proportional to dI/dt and is thus generally negligible except during the initial breakdown phase. Integration of Eq. (10) is straightforward, and for the kinetic energy T of the runaway we thus obtain

$$\frac{T}{m_o c^2} = \gamma - 1 = \sqrt{1 + \left(\frac{e}{m_o c^2} A_\phi\right)^2} - 1 \quad . \tag{12}$$

III. RUNAWAY ENERGY

High energy runaway electrons in ORMAK discharges can be lost to the limiter either

1) at the very beginning,

2) during the current plateau phase, or

3) when the current decays, as documented in Fig. 3.

In many cases, the runaway loss to the limiter is smooth and steady and can be described with surprising accuracy with the drift orbit model. In other cases, characterized by a noticeable MHD activity in the discharge, runaway losses to the limiter are somewhat enhanced and are in phase with the MHD surface effects. Strong disruptive instabilities may also dump most or even all of the runaways in the discharge.

Energy spectra of runaway electrons have been studied for different discharge types and different intervals within one discharge. Instead of following the direct double unfolding procedure necessary to determine the electron energy distribution from the scintillation pulse height spectrum, we assume some discrete electron energies and compare the resulting scintillation spectra with the experimental ones.[5] The results given in Fig. 4 show that substantial 10-MeV runaway components exist in such discharges. It is also apparent that because the highest energy runaways produce copious bremsstrahlung quanta over the whole spectrum, it is nearly impossible under these circumstances to obtain any useful information relative to the lower energy ($\lesssim$2-MeV) electrons.

For normal ORMAK discharges, there are two distinct patterns of runaway loss associated with different density regimes. For the high density case ($\bar{n}_e \gtrsim 2 \times 10^{13}$ cm^{-3} at $\approx$100 kA), the only runaway loss occurs during the current rise phase. For the low density case ($\bar{n}_e < 2 \times 10^{13}$ cm^{-3} at $\approx$100 kA), the main loss occurs during the steady-state and decay phases. (For the intermediate density case, both patterns can occur in the same discharge.) In either case, however, the maximum energy is seen to increase in time to nearly 10 MeV, over a period of $\lesssim$10 msec during the initially high loop voltage or over a period of $\lesssim$50 msec during the lower voltage in the steady state.

The knowledge of the maximum energy of the runaways on impact with the limiter can, through use of the model described in Sec. II, provide useful information concerning the radial distribution and acceleration of this group of runaways. The relevant maximum energy is deduced from the high energy end of the measured x-ray spectrum through a procedure similar to that shown in Fig. 4.[10]

A. Runaways lost at early times

A straightforward and interesting experimental result based on this simple but effective diagnostic method is shown in Fig. 5. The evolution of the maximum energy at early times is compared with free-fall curves; this shows that the corresponding electrons must have been generated at $t_R \simeq 0.4 \pm 0.4$ msec, at a time when the discharge is still cold (1-5 eV) and only partially ionized. They are then accelerated nearly as free electrons in the applied loop voltage V_L of 3-40 V per turn (Fig. 3). The mean line-averaged electron density at full ionization is relatively high in these shots, $\bar{n}_e$ = 2.5-3.5 $\times$ 10^{13} cm^{-3} at 5 msec. It is therefore no surprise that the overall number of high energy runaways is relatively small, typically N_R = 10^{12} electrons or a 10-A circulating current. An analysis of the orbits of these electrons through Eq. (8) shows that their minor radii are in the range r_c = 17-19 cm when intersecting the outer limiter. This result suggests the existence of a skin effect for electric field penetration (see Sec. V). It is also possible that in these discharges, characterized by a moderate MHD activity at early times, runaways are transported somewhat by ergodic wandering of the field lines. This effect is small enough, however, to allow nearly perfect confinement of runaways over the whole current rise phase.

It should be noted that in this series of experiments, the discharge is leaning towards the inside limiter, leaving space for shifted high energy electron orbits of large radius to remain contained. As a matter of fact, if the discharge in this early phase were leaning towards the outside limiter, as is typical of most ORMAK discharges, the energy of the same runaways at collision with the limiter would have been only 50-100 keV.

It is most likely that runaway formation during breakdown is not limited only to those documented ORMAK discharges, but is typical of most tokamak operations. For reasons just mentioned, peripheral runaways will, however, be mostly lost to the limiter or the wall before gaining relativistic energies. This effect has qualitatively been confirmed by pulses of soft and medium x ray that have been detected at these early times whenever we looked for them.

B. Runaways lost during steady state

For discharges with mean electron densities $(\bar{n}_e)$ of 0.5–2.0 × 10^{13} cm^{-3}, large numbers of runaway electrons are generated after t ≃ 5 msec and accelerated to high energies. They then gradually drift into the limiter from about mid-discharge on, with particularly large numbers being lost during current decay.

Maximum energy is plotted vs time for two sets of discharges in Fig. 6; the points have basically the same meaning as in Fig. 5. Since the electrons in Fig. 6 are accelerated more slowly during this phase of the discharge and are contained longer, the interpretation of their confinement is more open to discussion.

The points along curve (a) in Fig. 6 follow the free-fall slope within 90% ± 10% in such a way that if free fall is assumed also for E < 5 MeV their birthtimes would be ≈10 msec. The radii of the measured runaways along this curve as computed from the orbit model range from 16 to 19 cm. Along with an estimate of the absolute runaway loss, as shown at the bottom of the figure, this gives a local density of ≈10^7 cm^{-3} for these runaways.

Although such near-free-fall behavior has been seen in most cases, the energy gain can sometimes be smaller, as shown, for example, by curve (b). Here the energy gain is 60% ± 10% of free fall. At present, there is no convincing explanation for this result, although the most likely causes are an anomalous friction or an enhanced radial diffusion rate. Note that a time- or radius-dependent friction cannot be ruled out for runaways below 5 MeV in curve (a) and could place their birthtime anywhere between 0 and 10 msec.

C. Runaways lost at current decay

After the driving voltage ends, the discharge current starts decaying. As a consequence of the increased orbit shift [see Eq. (5)], all the runaways will eventually hit the limiter. The results plotted in Fig. 7 show that the energy and intensity can be consistently understood in terms of the drift orbit model. In particular, the strong increase of bremsstrahlung at the outer limiter when the current starts decaying is

obtained because the current decay term in Eq. (5) is much larger than the inward plasma shift which occurs at this time (see Fig. 6). Note that the last runaways to be dumped have smaller radii and lower energies, as would be expected for runaways born later in the hot central core of the discharge. Note also that in the high current discharge described in Fig. 7, runaways are dumped relatively late in time. Generally, the higher current discharges show better runaway confinement during the steady state and also a larger dump during the later phases of the current decay. This behavior is consistent with the 1/I scaling implied by the drift orbit model of confinement.

The total number of high energy runaways shown in Fig. 7 amounts to 10^{13} or an equivalent current of roughly 100 A for the sum of these maximum energy components. The uncertainty in this number, which is calculated on the basis of the absolute bremsstrahlung intensity, is a factor of three either way. In other similar shots the number can be substantially higher, depending on the plasma density (as discussed in Sec. V).

In ORMAK, the transformer providing the electromotive force (emf) is driven by a capacitor bank for the first 15 msec. When this time has elapsed, a lead cell battery is usually switched in to keep the discharge current at a constant level. In the series of experiments represented in Fig. 8, only the capacitor bank was used, and the capacitor voltage V_c was varied to change the overall flux swing ϕ within the discharge vessel. Each point in the figure thus corresponds to the runaway behavior observed for a particular charging voltage. The measured maximum energies can be shown to follow the free-fall gain if the runaways are all started at $t_o \cong 3$ msec, thus allowing them to miss a fraction of the flux swing.

As before, the results leave some room open for speculation as to what happens to the maximum energy runaways before they become detectable, that is, below 2 MeV. For example, it is possible that electrons start near $t_o = 0$ msec but their energy gain in the first few milliseconds of their lifetime is reduced by enhanced friction. It is clear, however, that the late dump (and thus the small calculated orbit radii) of these runaways distinguishes them from the group of breakdown runaways obtained at higher densities (see Sec. III.A).

We note two interesting features of this result with respect to runaway production. First, for the group of discharges at 0.09 Wb in Fig. 8, the preionization pulse amplitude was varied appreciably with apparently no systematic effect on either the maximum energy or intensity of the high energy runaways. Second, the number of high energy runaways is seen to decrease with increased voltage. This unexpected behavior (see Sec. V) is due to the dependence of n_e (and probably T_e) on the applied voltage (see Fig. 8) and points out the difficulty of predicting runaway production in tokamak discharges.

Finally, it may be interesting to note that in an additional series of experiments the flux swing range was further extended up to 0.8 Wb by switching the battery into the transformer circuit for various lengths of time. In these experiments the maximum energy of runaways dumped at the end of the discharges increased at only one third the rate expected from free fall in the extra flux swing. No clear-cut explanation can be given for this effect. It is possible, though, that the runaways did continue in free fall, but their population was not detectable in the presence of a large number of runaways born later.

IV. RUNAWAY TRANSPORT

A. Overall transport properties

Runaway electrons become relativistic after they have passed through several initial phases in their lifetime. Three major phases can be defined by critical energy ranges. The first concerns the runaway birth and can be defined by $T < W_1$, where typically $W_1 \simeq 2eE_c c/\nu_{ei}$ is on the order of the critical runaway energy, implying that at W_1 the runaway becomes decoupled from the plasma. Here ν_{ei} is the collision frequency and E_c is given in Eq. (14); thus for a normally hot plasma ($n_e = 3 \times 10^{13}$ cm^{-3}, $T_e = 1$ keV), we obtain $W_1 \simeq 40$ keV. In this phase, the generation of runaways and the friction experienced by recently born runaways may be mostly determined, in addition to Coulomb collisions, by collective interaction modes. This may result in a reduced number of runaways and in pitch angle scattered or slowed-down runaways on one hand

and in emission of enhanced electron synchrotron and plasma radiation on the other.[3,11] Correlation between runaway effects and enhanced high frequency radiation has been detected in many experiments[12] and also in ORMAK.[13] In this phase an enhanced transport of runaways may be related to the anomalously large electron energy loss characteristic of tokamak discharges.

The second phase may be defined by the kinetic energy interval (W_1, W_2). Here W_2 is the energy at which the orbit shift d_γ [Eq. (5)] typically becomes equal to the radial thickness Δr_m of defects in the magnetic configuration (in ORMAK, at half radius with $\Delta r_m \simeq 1$ cm, we have $W_2 \simeq 1$ MeV). In this phase, the drift velocity of runaway electrons along magnetic field lines is typically larger by a factor of 100 than that of the bulk of electrons carrying current; thus the runaway electrons sense dramatically any ergodicity of the magnetic topology. Relatively large runaway losses measured[14] in smaller plasmas than ORMAK's could be due to this effect. Very small magnetic perturbations ($\tilde{B}/B \gtrsim 10^{-4}$), which can be induced by experimentally observed drift waves ($e\tilde{\phi}/kT_e \sim 10^{-2}$),[15] can thus enhance very substantially radial transport of runaways in this energy range.

In addition, major defects in the smooth magnetic topology, such as islands along mode rational surfaces, internal sawtooth oscillations, or disruptions, can affect the radial transport of runaways much more than in the previous case. In fact, detailed correlation between such activities (measured by magnetic probes or by a positive-intrinsic-negative diode array sensitive to soft x rays) and the hard x-ray signal at the limiter has repeatedly been measured.[10]

Finally, for kinetic energies larger than W_2, the drift surfaces decouple partially from the magnetic flux surfaces, and the inertia of the electrons increases by the factor γ. The runaways are less affected by small-scale and resonant effects, and their confinement time can greatly exceed the electron energy containment time, as shown by our experiments. For example, in the discharges described in Secs. II.B and II.C, the high energy runaway containment time can exceed 50 msec, while the electron energy confinement time is typically $\lesssim 5$ msec.

B. Normal limiter-target effects

According to our model, under normal discharge conditions the high
energy runaways move on orbits that are always shifted outward along
the major radius with respect to the current distribution in the plasma.
The intensity plot given in Fig. 9a indeed shows a strong bremsstrahlung
source at the outer limiter and no clearly detectable source at the inner
limiter. (The remaining intensity roughly corresponds to the estimated
background of radiation that is Compton-scattered into the acceptance
cone of the collimator.)

A confirmation of the basic loss mechanism was found during inspec-
tion of the ORMAK limiter after more than three years of operation, during
which many series of runaway beam discharges were also sustained. The
main damage pattern that might be ascribed to impact of high energy
electrons is a slight melting at the outer limiter extending about 3 cm
up and down from the equatorial symmetry plane, that is, just where the
drifted and perfectly symmetric electron orbit should intersect the
limiter.

The very good containment of these high energy runaways within the
plasma makes it possible to shift their orbits in the machine along with
the plasma by changing the vertical field. If the orbits are shifted
inward (as, for example, in Fig. 5), the runaways are allowed to gain
more energy before hitting the limiter. A series of such shift experi-
ments[10,13] as well as the similar experiment documented in Fig. 5
substantially confirm the drift orbit model. Recent experimental results
show that in addition to the velocity $\Delta d_\gamma/\Delta t$ with which the drift surfaces
shift into the limiter [for which from Eq. (9) a typical value is found
to be 10^2 cm/sec], an additional (formal) diffusion process with $d \approx 10^2$
cm^2/sec can be allowed. This process increases somewhat the transport of
high energy runaways near the outside of the discharge where, in fact,
additional effects may play a role (see Sec. IV.A).

C. Point limiter effects

A further test of the validity of the drift orbit model was made with
an experiment in which an additional movable limiter in the form of a

1-cm-diam tungsten rod was radially pointed into the discharge chamber in the equatorial plane (see insert, Fig. 9b). As this limiter was gradually inserted over a series of shots, the hard x-ray intensity at the outer section of the ordinary limiter, measured in the usual way, was found to decrease correspondingly (Fig. 9b); however, the intensity at the inner section of the limiter, lower by about a factor of 100, remained roughly constant during such runs. The intensity at the outer limiter was seen to decrease gradually over an insertion distance of $\lesssim 2$ cm, as shown in Fig. 9b.

In addition, the movable limiter, upon removal after about 30 discharges, showed a damage pattern consistent with high energy electron impact (see insert, Fig. 9b). In particular, the flat surface facing the plasma was not damaged, as it would have been if the overall limiter damage were due to hot, normal conduction electrons or ions, or to runaways with a substantial radial velocity.

Both observations relative to the inserted movable limiter indicate that high energy runaways can move radially outward as much as $d_d \simeq 1.5$ cm past the tip of this limiter. To estimate the corresponding radial diffusion velocity v_r, we note that the ideal relativistic electron moving without transverse energy on an orbit with mean radius r_c is likely to hit the tungsten rod with diameter $2r_t$ only after $2\pi r_c/2r_t$ toroidal transits, each of which is completed in the time $2\pi R_o/c$; hence, $v_r = d_d(r_t/\pi r_c)(c/2\pi R_o)$, so with $r_c \cong 18$ cm, it follows that $v_r \simeq 400$ cm/sec. It is obvious that this outward velocity could only be effective a short distance from the limiter, implying that this is a surface rather than a bulk phenomenon, because otherwise the mean lifetime of electrons would be much less than that required to gain relativistic energies.

There are several effects that can explain this enhanced diffusion. The most relevant with respect to the high energy runaway experiment reported in Fig. 9b is a scattering of the electrons as they hit the point limiter. In fact, as the runaways (initially with small transverse momentum) move outward with the slow drift orbit motion discussed in Sec. IV.B, they should eventually hit the point limiter within less than a millimeter of its tip. In such a collision, there is a good chance that the electron is not absorbed but is instead violently scattered. In a

plane tungsten target, for example, the backscattered fraction of normally incident 4-MeV electrons can be as high as 30%.[16] Electrons hitting a cylindrical limiter can, in addition, be scattered by the curved surfaces and also through the flat surface facing the plasma; it is estimated that 20-30% of these electrons will be nearly elastically scattered away from the limiter into gyro-orbits with a pitch angle of more than 20°. The main consequence of such collisions is that the orbit of the scattered electrons is displaced by a mean step corresponding to the Larmor radius [Eq. (1)] or more if the runaway becomes trapped (typically for scattering angles of more than 50°). On consequent passages they may hit the main limiter (with a chance of being detected and thus reported as in Fig. 9b), be scattered a second time, or be absorbed by the point limiter. This effect is somewhat difficult to express in exact quantitative terms, due to the complex geometry of the two targets, but since elastic scattering prevails so strongly over bremsstrahlung radiated into the detector's high energy acceptance range, there remains an ample margin to cover the experimental observations. Notice that a similar scattering effect also exists with only the normal limiter in place; however, due to its large poloidal extension, the radial displacement of runaway impact will be somewhat less pronounced.

V. RUNAWAY PRODUCTION

In recent years, an appreciable amount of theoretical and numerical work on runaway production rates has been presented, generally based on ideal plasma models and on Coulomb collisions only. However, these results are so critically and strongly dependent on some plasma parameters, such as electron density n_e and temperature T_e, and also on collective effects that have not been sufficiently taken into account, that at present some doubts exist about their applicability to real plasmas.

For the relative rate S/n_e of electrons running away per second in a fully ionized plasma, we take here for comparison with the experiments the result of Kulsrud et al.[17] and rewrite it in the approximate practical form

$$\frac{S}{n_e} \simeq 1.6 \times 10^9 \, \frac{(n_e/10^{13})}{T_e^{3/2}} \left(\frac{E_c}{E}\right)^{0.375} \quad \exp\left(-\frac{E_c}{4E} \sqrt{\frac{2E_c}{E}}\right) . \tag{13}$$

The characteristic runaway field

$$E_c = 4\pi e^3 \frac{n_e}{kT_e} \ln \Lambda \tag{14}$$

can be taken in the form (with $\ln \Lambda \simeq 15$)

$$E_c \simeq 4 \times 10^{-2} \left(\frac{n_e}{10^{13}}\right) \left(\frac{10^3}{T_e}\right) ,$$

where T_e is measured in eV, n_e in cm^{-3}, E and E_c in $V\text{-}cm^{-1}$.

There are at least three basic effects that modify the runaway rates in real plasmas with respect to what is given above. Probably the most general one is due to collective plasma modes (see Sec. IV.A).

The second effect concerns impurity ions in the plasma. According to an expression by Cohen,[18] in a typical ORMAK plasma ($E/E_c \lesssim 0.1$) with effective ionic charge Z = 6 in the steady-state phase, the runaway rate would be smaller by an order of magnitude than given by Eq. (13). On the other hand, impurities are known to indirectly enhance runaway formation, particularly in the strong runaway type of discharge, where runaway beams are formed at early times; this has reproducibly been checked in ORMAK.[9]

Finally, there is an enhancement of runaway formation obtained during breakdown[19] in the partially ionized gas; this is due to the intermixed molecular gas, which provides a collisional (momentum transfer) cross section per molecule that is smaller[20] than twice the corresponding electron-ion cross section in the electron energy range up to about 50 eV. The very early breakdown runaways documented in Fig. 5 are most likely generated through this enhancement effect. In fact, unless one assumes a pronounced skin effect with strong local heating, the high filling pressure and low initial temperature characterizing these discharges provide practically no detectable runaways through Eq. (13).

On the basis of this expression and of measured n_e, T_e, and E
values, a typical evolution in time and radius of runaway generation rates
in the ORMAK discharge is obtained in Fig. 10. It is clear that between
the "early" and "steady-state" runaways there is a period from about 10
to 20 msec during which runaway production is quenched because the
electric field has decreased more than the temperature has increased.
Another result is that at an early time ($\lesssim 5$ msec), as long as inductive
effects reduce the electric field inside the discharge, runaway produc-
tion may be higher at outer radii than in the center. With respect to
runaways generated after this time, Fig. 12 shows a drastic increase in
runaway intensity as the mean electron density (measured at 30 msec)
becomes smaller than about 1.3×10^{13} cm^{-3}. The comparison with the
relative theoretical curve shows that the experimental results can roughly
be understood in terms of the density dependence given by Eq. (13).

It is interesting to attempt a quantitative comparison between this
calculated runaway production and the observed population of high energy
runaways. It must be kept in mind, however, that our measurements refer
only to the highest energy components lost to the limiter at any time,
as shown, for example, in Figs. 6 and 7.

Because runaways with the largest energies are predominantly formed
in ORMAK at early times, we can compare the observed population of $\approx$10-MeV
runaways lost during the current decay to the expected number born at the
free-fall-extrapolated birthtime of t $\approx$ 10 msec. From Fig. 10 (corrected
for ORMAK Z = 6), we find an expected runaway production during this time
for a typical volume of $\gtrsim 10^5$ cm^3 to be $\gtrsim 10^{15}$ electrons. This can be
compared to the observed population of $\approx 10^{13}$ electrons for this density
(Fig. 11). Apparently, either the production rate is less than classical
or some of the runaways are lost before they reach maximum energy,
probably before becoming relativistic. It must be kept in mind, however,
that the uncertainties involved are at least a factor of three either way
for each figure.

In addition, a steady-state production rate is in part reflected in
the loss of lower energy components during the end of the current decay
as described in Sec. III.C. In the high current, high temperature
discharge of Fig. 7, this component evidently implies a significant

production rate in the steady state, but in this case an anomalous frictional force on earlier born runaways cannot be ruled out as an explanation for the relatively low energy.

In larger tokamaks,[1,2] this latter type of runaway may strongly predominate due to the increased time of the discharge pulse. A steady state in the population of runaway electrons in a discharge would be the result of a balance between runaway generation and loss; in general, these processes can be inferred only indirectly from experimental results. An enhanced loss rate for low energy runaway components can produce a similar result.[21]

VI. CONCLUSIONS

The experimental results presented and discussed in this work show that in a variety of normal ORMAK discharges, runaway electrons can be accelerated as (nearly) free electrons up to maximum energies of 10 MeV. They thus pass through the lower energy range (≤ 0.5 MeV) where they are critically exposed to collective plasma modes and defects of the magnetic topology.

A variety of indirect observations suggest that the dynamics of these high energy runaways can basically be understood in terms of a simple physical model. In particular, the surprisingly good confinement (for times of over 50 msec for the higher energy components) which exists in spite of the complex oscillating magnetic topology of tokamaks may be hypothesized as being due to the sizable shift of the drifted orbits away from the magnetic flux surfaces.

The group of high energy runaways can influence the physics and the macroscopic characteristics of tokamak discharges, particularly at early times. For example, the early enhanced runaway formation should in most cases give rise to an unstable positive slope in the electron distribution which would tend to produce a wave spectrum. This wave spectrum would self-consistently determine further runaway production and acceleration. Also, due to the electron stimulated desorption,[22] this early runaway dump might cause influx of neutral gas and thus help to determine the character of the discharge. High energy runaways also have several important

practical consequences later in the discharge, such as the generation of large fluxes of penetrating hard x-rays that interfere with many diagnostic systems, the generation of neutrons by photoreactions in the limiter material and/or by Coulomb dissociation of deuterium in the plasma, and possibly the enhancement of high Z impurity influx due to runaway induced evaporation of the limiter. One of these effects, anticipated earlier[4] on the basis of our results, has meanwhile been detected and studied in detail.[23]

The study of high energy electrons has allowed us to identify several distinct groups of runaways that can be classified in accordance with the time and condition of birth. In this sense the runaway population, as inferred from high energy results, qualitatively agrees with the theoretical runaway rate, but quantitatively tends to be more than an order of magnitude smaller than calculated.

In conclusion, considering the physical complexity of runaway phenomena in tokamak discharges, it can be seen that high energy runaway effects are remarkably reproducible and controllable.

REFERENCES

* On leave from Centro Gas Ionizzati (Associazione EURATOM-Comitato Nazionale Energia Nucleare), Frascati, Italy.

† Oak Ridge Associated Universities graduate participant from Cornell University, Ithaca, New York.

1. D. Grove, V. Arunsalam, K. Bol, D. Boyd, N. Brentz, M. Brusati, S. Cohen, D. Dimock, F. Dylla, D. Eames, H. Eubank, B. Fraenkel, J. Girard, R. Hawryluk, E. Hinnov, R. Horton, J. Hosea, H. Hsuan, D. Ignat, F. Jobes, D. Johnson, E. Mazzucato, E. Meservey, N. Sauthoff, J. Schivell, G. Schmidt, R. Smith, F. Stauffer, W. Stodiek, J. Strachan, S. Suckerwer, S. von Goeler, and K. Young, paper CN-35/A2 in Proc. 6th Conf. on Plasma Physics and Controlled Nuclear Fusion Research (1976).

2. A. B. Berlizov, C. A. Bobrovskii, A. A. Bagdasarov, N. L. Vasin, A. N. Vertiporokh, V. P. Vinogradov, N. D. Vinogradova, N. M. Gegechkory, E. P. Gorbunov, Yu. N. Dnestrovskii, V. S. Zaverjaev, A. B. Izvozchikov, S. Yu. Luk'anov, S. E. Lysenko, Yu. S. Maximov, G. E. Notkin, M. P. Petrov, G. N. Popkov, K. A. Razumova, V. S. Strelkov, and D. A. Shcheglov, paper CN-35/A1, in Proc. 6th Conf. on Plasma Physics and Controlled Nuclear Fusion Research (1976).

3. B. Coppi, F. Pegoraro, R. Pozzoli, and G. Rewoldt, Nucl. Fusion 16, 309 (1976).

4. H. Knoepfel and S. J. Zweben, Phys. Rev. Lett. 35, 1340 (1975).

5. H. Knoepfel, T. Renk, and S. J. Zweben, ORNL/TM-5022, Oak Ridge National Laboratory, Oak Ridge, Tennessee (1975).

6. J. L. Anderson, R. S. Booth, R. J. Colchin, R. V. Miskell, and J. M. Bailey, Nucl. Fusion 16, 629 (1976).

7. D. A. Spong and D. W. Swain, Bull. Am. Phys. Soc. 22(2), 182 (1977).

8. H. Knoepfel, D. A. Spong, and S. J. Zweben, Proc. 7th European Conf. on Controlled Fusion and Plasma Physics, Vol. I, p. 3 (1975).

9. H. Knoepfel, D. A. Spong, and S. J. Zweben, Phys. Fluids 20, 511 (1977.)

10. S. J. Zweben, Ph.D. dissertation, Cornell University, Ithaca, New York (1977).

11. For example, in C. S. Liu and Y. Mok, Phys. Rev. Lett. $\underline{38}$, 162 (1977); K. Papadopoulas, I. Haber, J. Huba, P. Palmadesso, and N. Winsor, Bull. Am. Phys. Soc. $\underline{22}$(2), 184 (1977).

12. For example, in D. A. Boyd, F. J. Stauffer, and A. W. Trivelpiece, Phys. Rev. Lett. $\underline{37}$, 98 (1976).

13. S. J. Zweben, D. W. Swain, J. B. Wilgen, and H. H. Fleischmann, Bull. Am. Phys. Soc. $\underline{22}$(2), 182 (1977).

14. J. D. Strachan, Nucl. Fusion $\underline{16}$, 345 (1976).

15. J. D. Callen, to be published.

16. P. J. Ebert, A. F. Lawson, and E. M. Lent, Phys. Rev. $\underline{138}$, 422 (1969).

17. R. M. Kulsrud, Y. C. Sun, N. K. Winsor, and H. A. Fallon, Phys. Rev. Lett. $\underline{31}$, 690 (1973).

18. R. H. Cohen, Phys. Fluids $\underline{19}$, 239 (1976).

19. R. Papoular, Nucl. Fusion $\underline{16}$, 37 (1973).

20. H. S. W. Massey and E. H. S. Burhop, Electronic and Ionic Impact Phenomena (Clarendon Press, Oxford, 1969), Vol. II.

21. S. von Goeler, W. Stodiek, N. Sauthoff, and H. Selberg, Proc. 3rd Intl. Symposium on Toroidal Plasma Confinement (1975), p. B25.

22. S. K. Erents and G. M. McCracken, J. Appl. Phys. $\underline{44}$, 3139 (1973).

23. J. D. Strachan, E. B. Meservey, W. Stodiek, R. A. Naumann, and F. Girshick, Nucl. Fusion $\underline{17}$, 140 (1977).

FIGURE CAPTIONS

Fig. 1.   Schematic cross section through an ORMAK discharge, where R_o = 80 cm and r_L = 23 cm.   A runaway drift surface AB is shown shifted outward d_γ from a magnetic flux surface which is itself shifted d_p inside the chamber axis.

Fig. 2.   Outer limiter intersection condition as a function of total plasma current (I) and electron energy (I_A).   The "filament" current curve corresponds to Eq. (8), the "flat" curve to uniform current density, and the "type B" curve to the current distribution of Eq. (7).   Insert shows calculated orbit with 100 kA of "type B" current for 5-MeV (outer) and 10-MeV (inner) electrons.

Fig. 3.   Hard ($\geq$0.5-MeV) x-ray intensity signatures for different types of ORMAK discharges as monitored by an uncollimated NaI detector. In discharges of intermediate density both the early and late x-ray signals may appear in the same discharge.

Fig. 4.   A typical scintillator pulse height spectrum matched with theoretical curves.   The histogram represents data obtained during a 5 msec interval summed over four similar discharges (90-95 msec in Fig. 7).   The solid curve is the expected spectrum for 0° emission from 2×10^{11} 10-MeV electrons normally incident on tungsten.   The broken curve includes an additional component of 4×10^{11} electrons at 5 MeV.

Fig. 5.   Early time evaluation of the maximum runaway energy in two sets of discharges.   The curves represent free-fall energy gain from t = 0 assuming an L $\cong$ 0.5 μH appropriate for electrons at approximately $r_c \gtrsim$ 18 cm. Plasma current and shift curves are given for the 90-kA case.

Fig. 6.   Maximum energy vs time for runaways hitting the limiter during the steady state of two discharges.   Plasma current, plasma shift, number of electrons lost, and typical orbit radii are shown for the (a) discharge.

Fig. 7. Maximum energy and intensity of runaways hitting the limiter during the discharge current decay. The number of runaways lost and the calculated orbit radii are computed for the energy components shown at the top of the figure.

Fig. 8. Maximum energy vs total flux swing for a series of discharges in which the capacitor charging voltage V_c was varied. Also shown is the variation in plasma density and in the estimated number of high energy runaways during this sequence.

Fig. 9a. Relative bremsstrahlung intensity (number of pulses above a threshold of 2 MeV) measured by the collimated detector as it sweeps in the equatorial plane from the inner to the outer limiter. The FWHM of the collimator's acceptance cone measured at the limiter is 6 cm.

Fig. 9b. Relative bremsstrahlung intensity measured at the outer limiter for various insertion distances of the point limiter. The melting of the point limiter is due to runaway impact.

Fig. 10. Runaway rate S for a pure hydrogen plasma calculated vs time and radius from measured density and temperature profiles in ORMAK. The electric field is calculated from the loop voltage, using $L = 0.5$ μH for the outside ($r \cong 15$ cm) and $L = 0.9$ μH for the inside ($r \cong 0$). Note that the steady-state rate is more commonly higher on axis due to a peaked temperature profile.

Fig. 11. Relative intensity of high energy ($\gtrsim 2$-MeV) runaways from three different experimental series vs mean electron line density. Solid line is obtained from Eq. (13) with $T_e = 500$ eV and $E = 7 \times 10^{-3}$ V/cm and is normalized at $\bar{n}_e = 1.2 \times 10^{13}$ cm^{-3} with the experimental points. Note that these data refer to runaways lost during the steady-state and current decay phases of the discharge, and so describe runaway production characteristic of $t \approx 5$-15 msec.
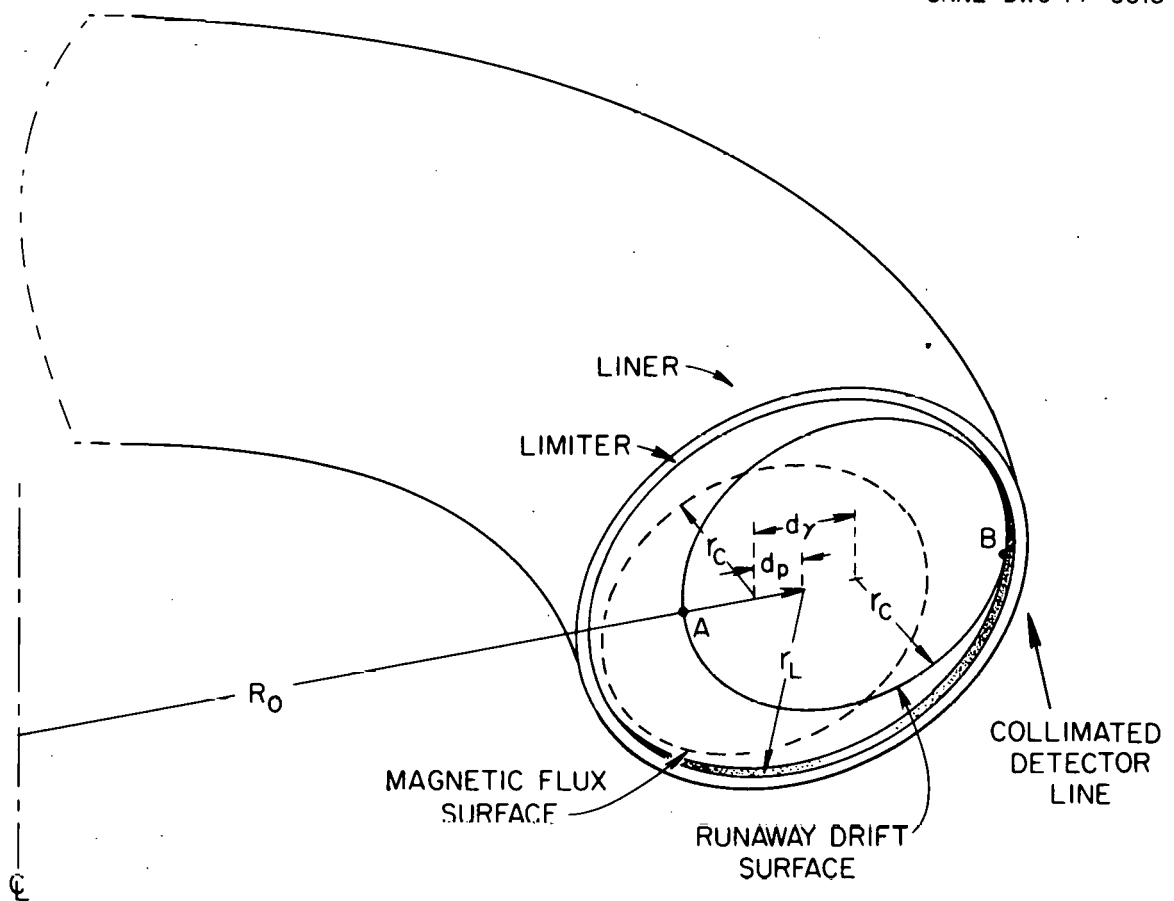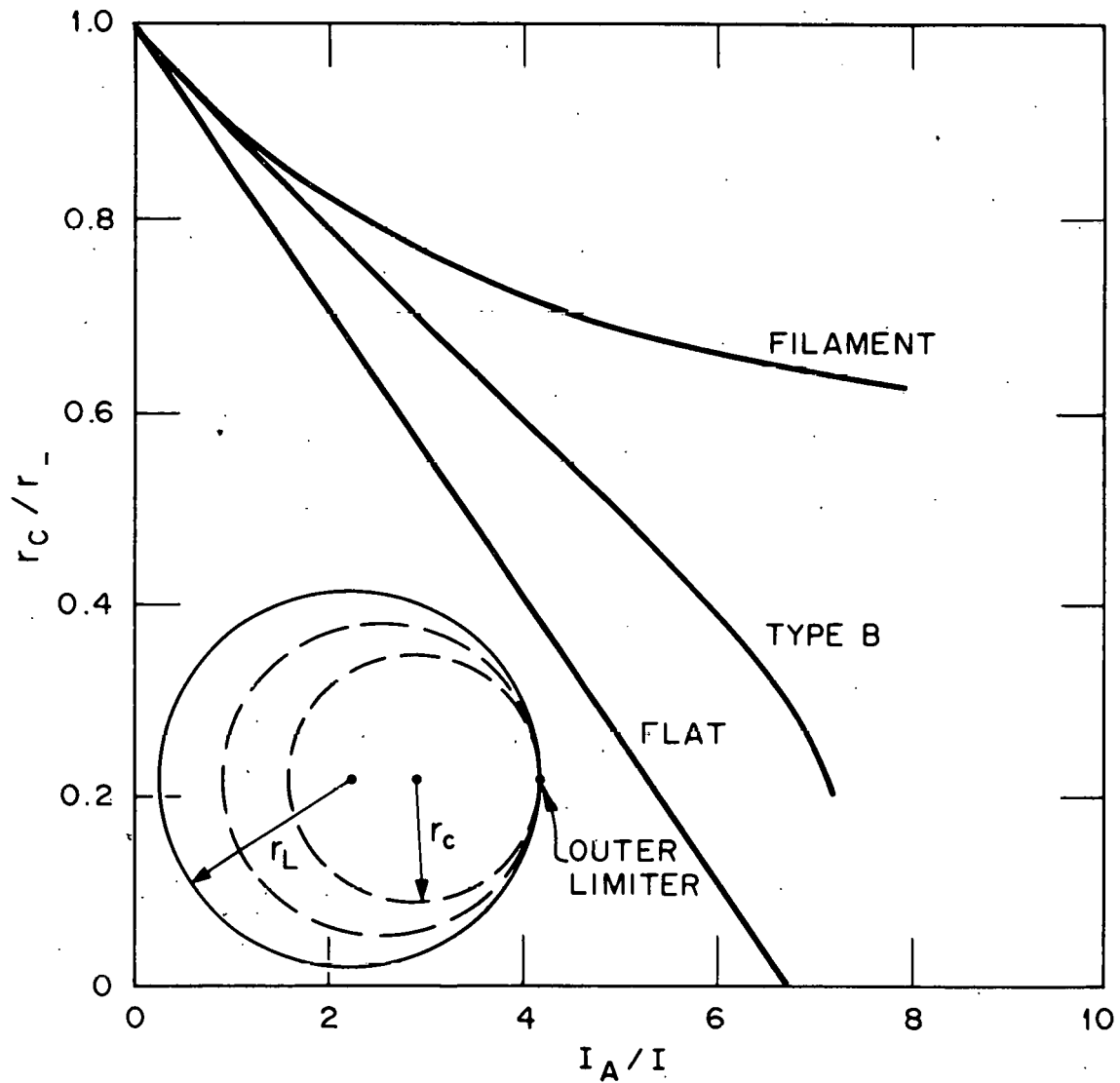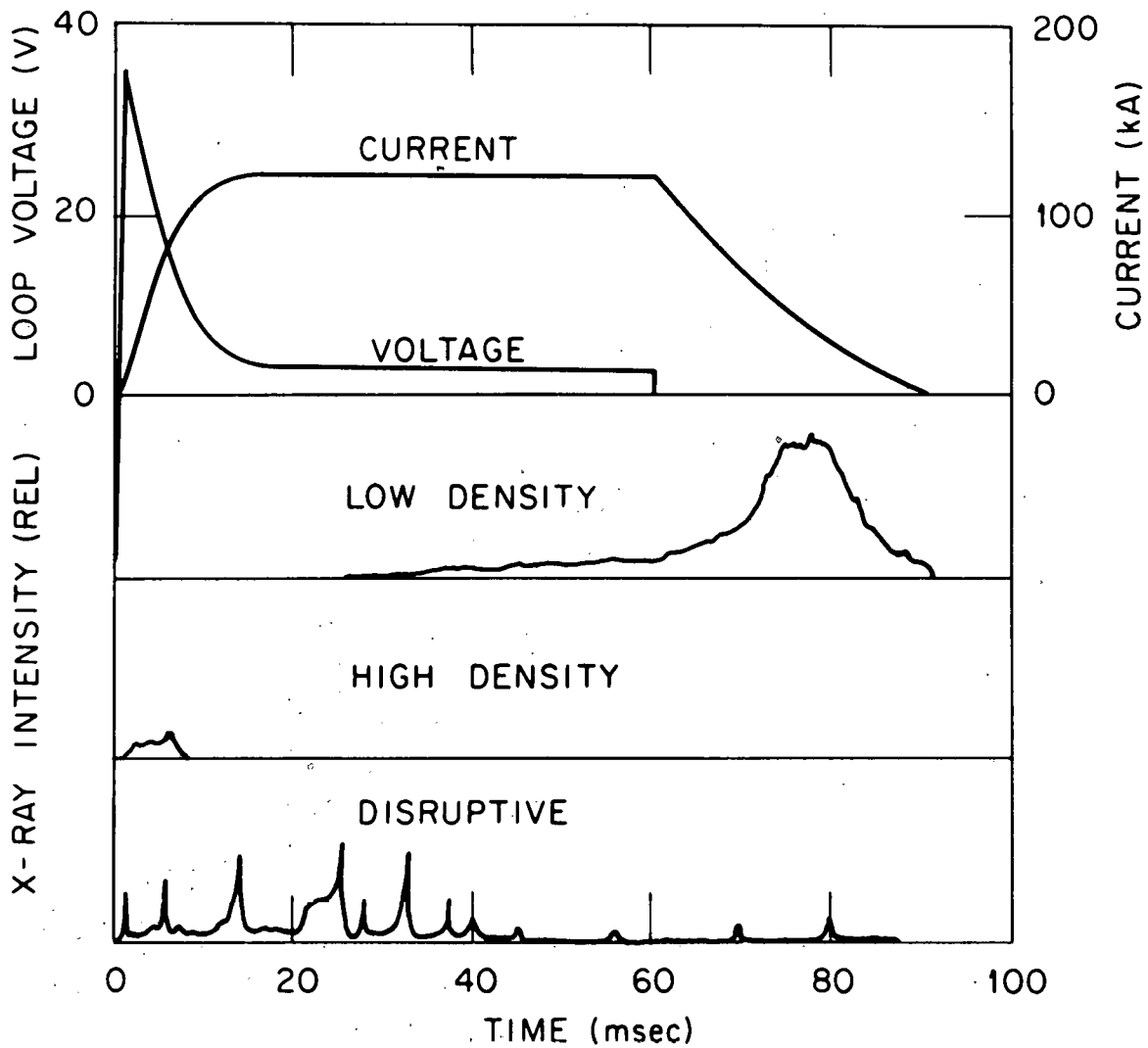
ORNL-DWG 77-5013

Fig. 1.

ORNL-DWG 77-3701R
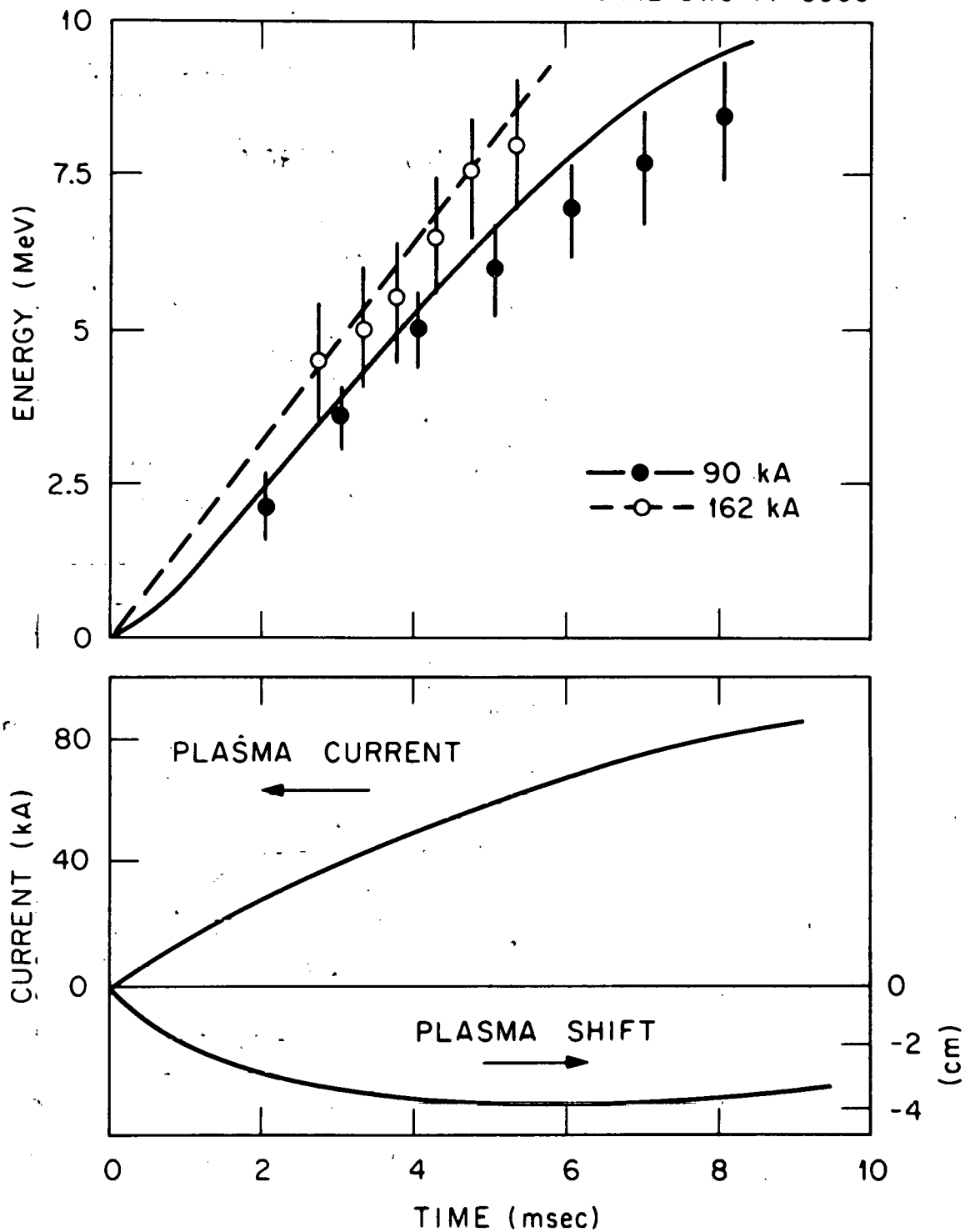

Fig. 2.

Fig. 3.

ORNL-DWG 77-5005

Fig. 4.

ORNL-DWG 77-5006
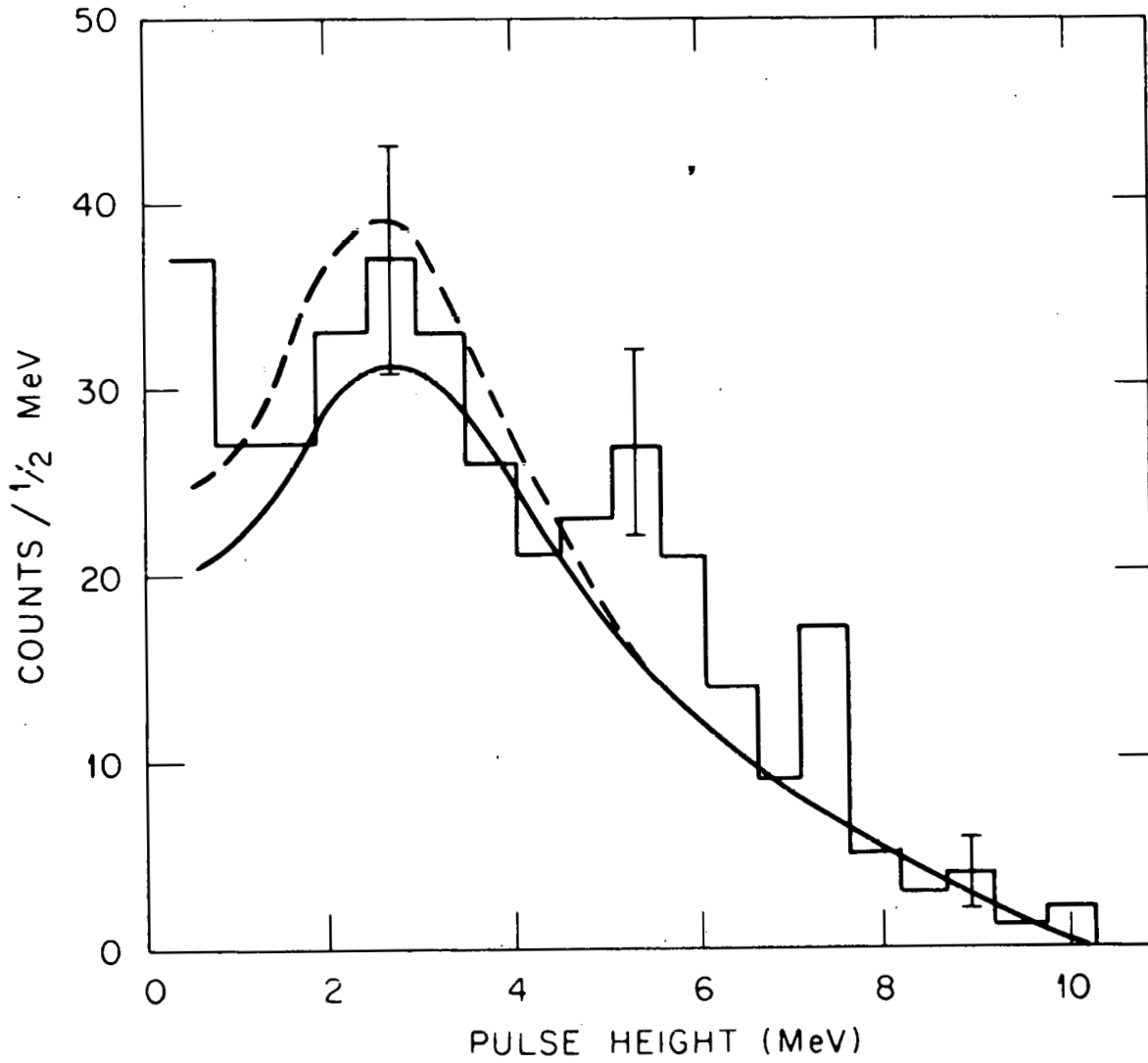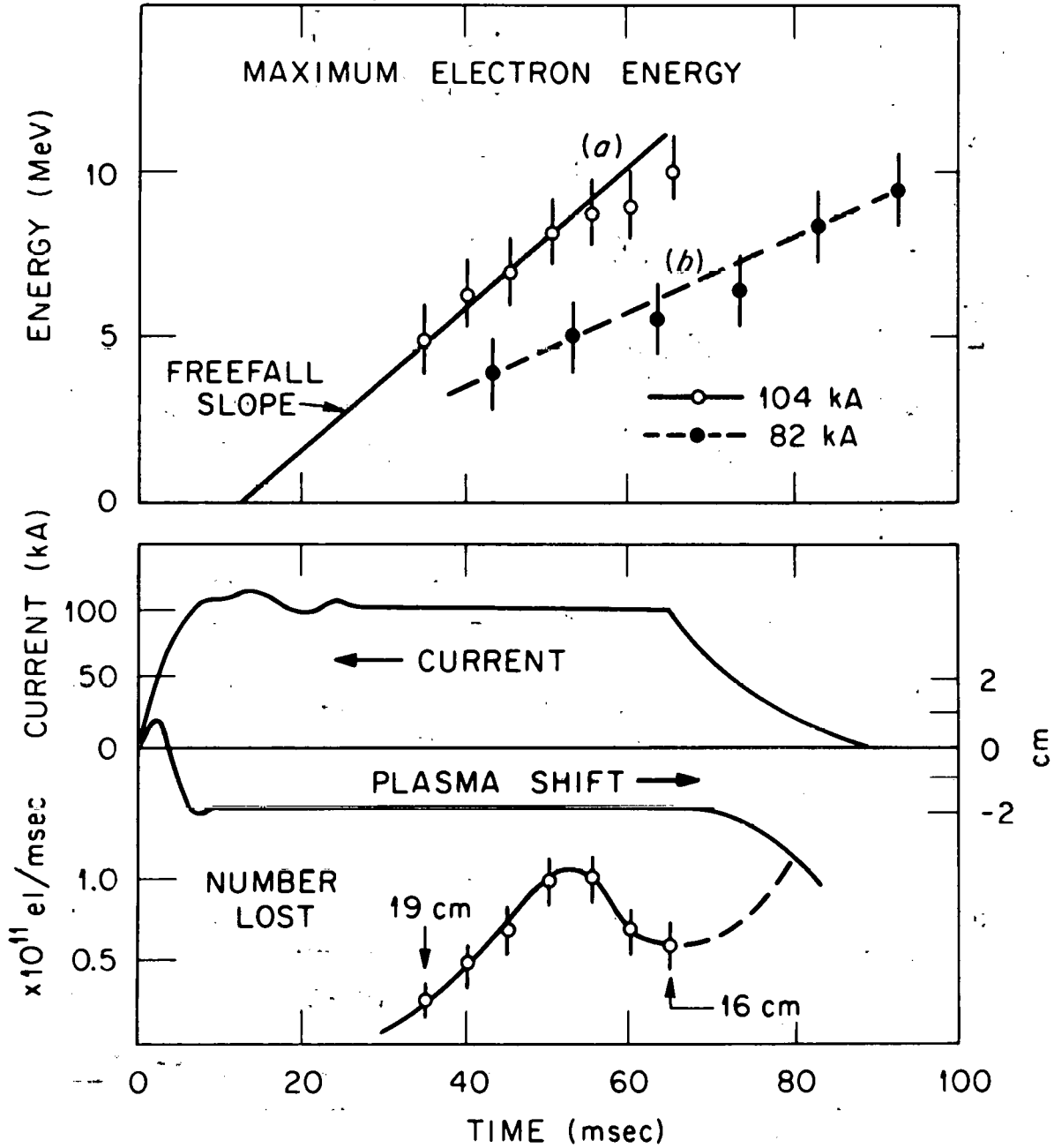

Fig. 5.

ORNL-DWG 77-5010

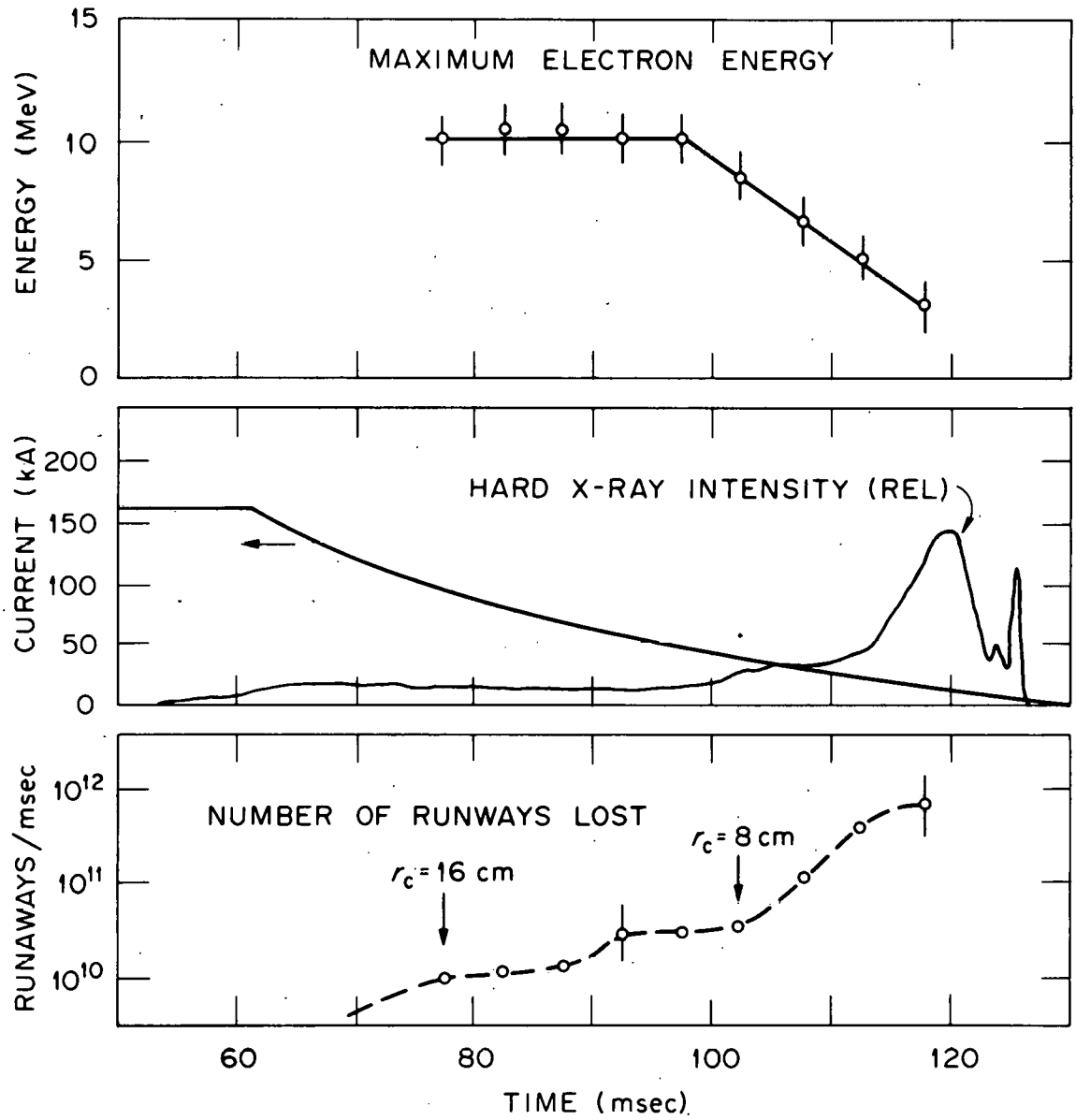

Fig. 6.

ORNL- DWG 77-5007R
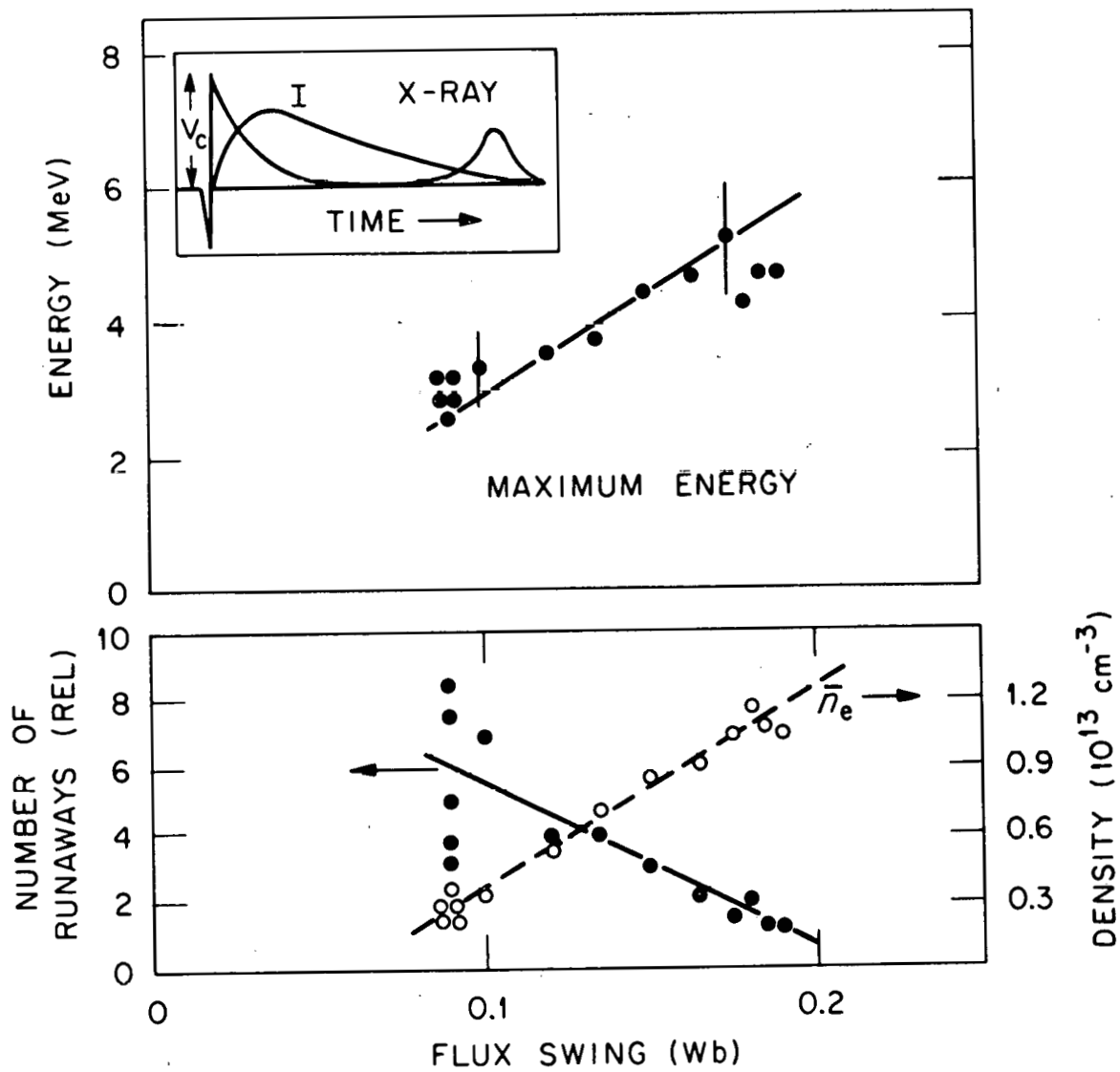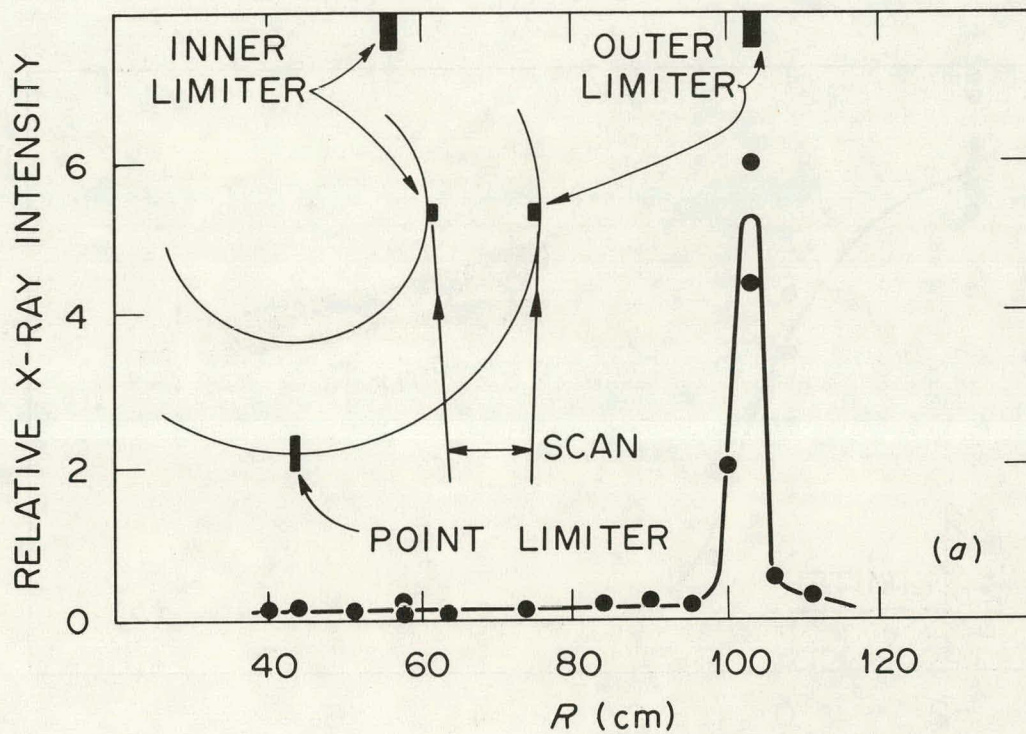

Fig. 7.

ORNL- DWG 77- 5008

Fig. 8.

ORNL-DWG 77-5012
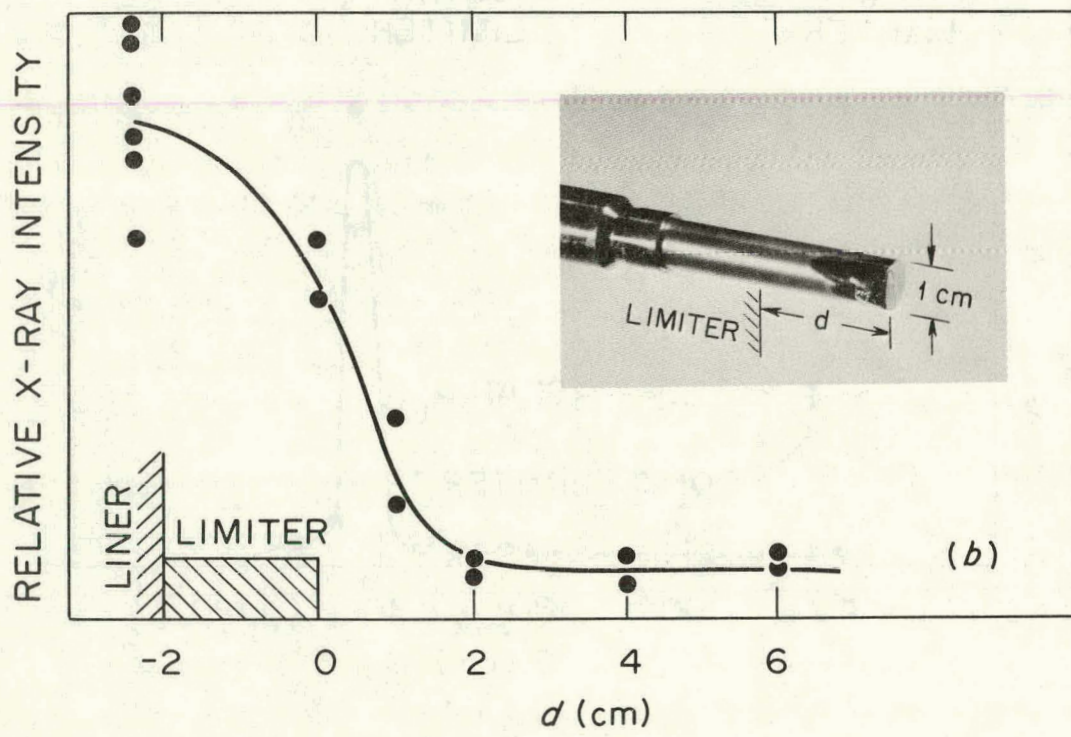

Fig. 9a.

ORNL—DWG 77—5012

Fig. 9b.

ORNL-DWG 77-5009

Fig. 10.

ORNL-DWG 77-5011
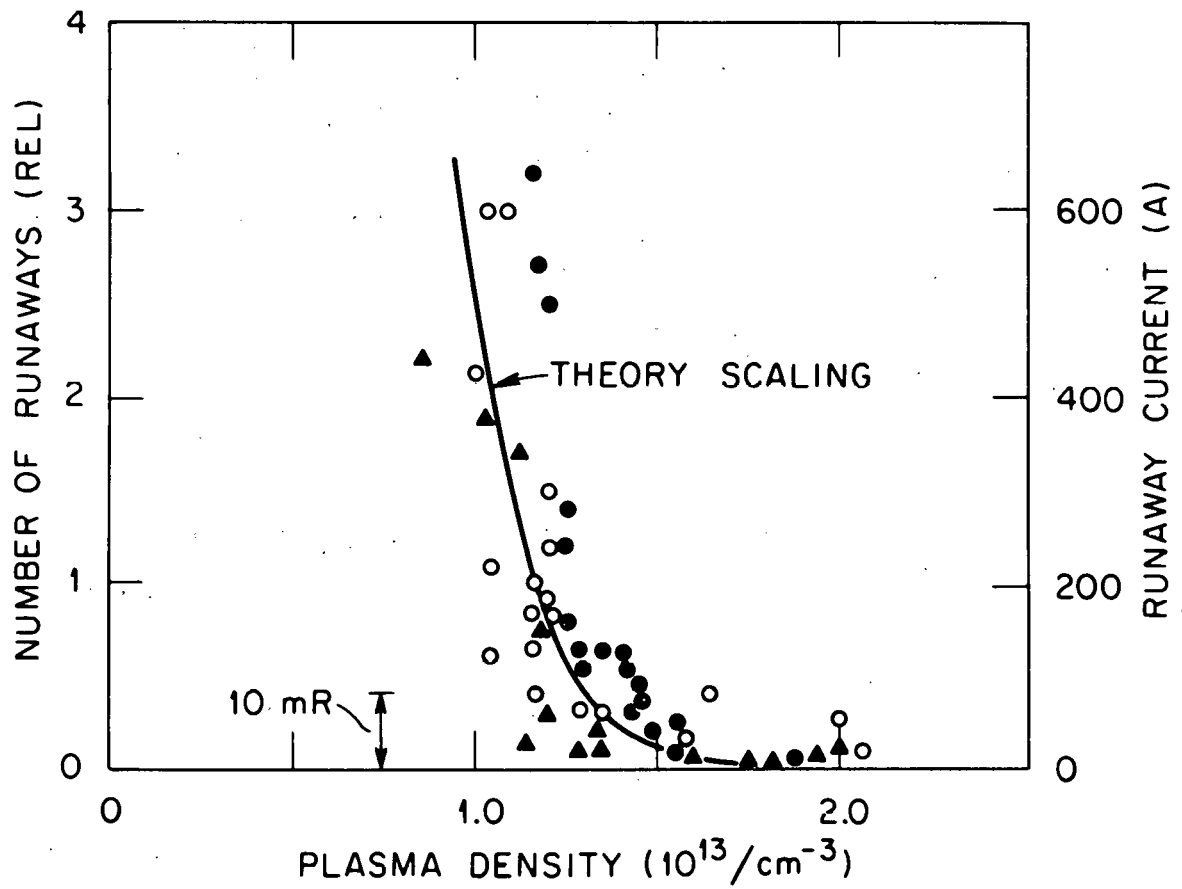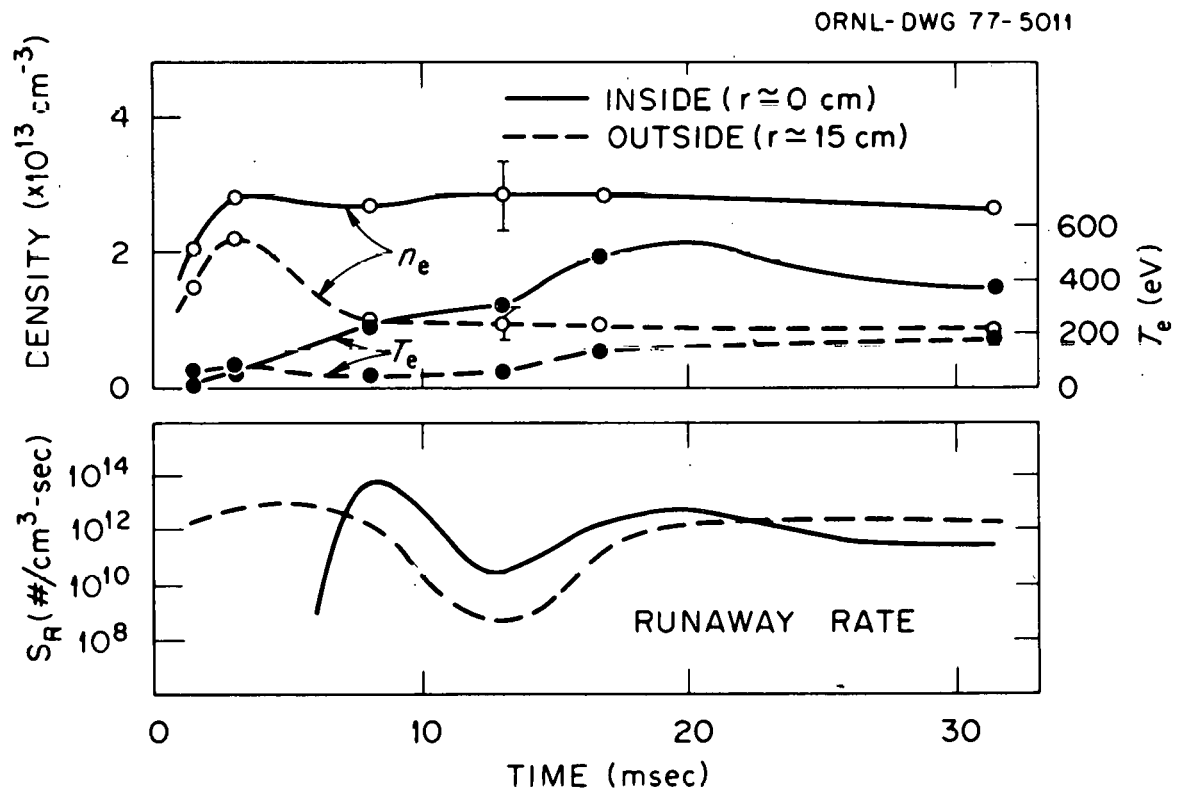

Fig. 11.

INTERNAL DISTRIBUTION

1.	L. A. Berry	21.	M. Murakami
2.	C. E. Bush	22.	W. Namkung
3.	J. D. Callen	23.	R. V. Neidigh
4.	R. J. Colchin	24.	G. H. Neilson
5.	A. C. Cooper	25.	V. K. Paré
6.	L. Drooks	26.	J. A. Rome
7.	J. L. Dunlap	27.	D. A. Spong
8.	P. H. Edmonds	28.	D. W. Swain
9.	A. C. England	29.	B. V. Waddell
10.	J. T. Hogan	30.	J. B. Wilgen
11.	H. C. Howe, Jr.	31.	W. R. Wing
12.	R. C. Isler	32-33.	Central Research Library
13.	T. C. Jernigan	34.	Document Reference Section
14.	G. G. Kelley	35-36.	Laboratory Records Department
15.	H. E. Ketterer	37.	Laboratory Records, ORNL-RC
16.	P. W. King	38.	ORNL Patent Office
17.	R. Langley	39.	Fusion Energy Division Library
18.	J. F. Lyon	40.	Fusion Energy Division Reports
19.	D. McNeill		Office
20.	J. T. Mihalczo		

EXTERNAL DISTRIBUTION

41. V. V. Alikaev, Kurchatov Institute of Atomic Energy, 46 Ulitsa Kurchatova, P.O. Box 3402, Moscow, U.S.S.R.
42. J. Bauer, General Atomic Co., P.O. Box 81608, San Diego, CA 92138
43. Bibliothèque, Service du Confinement des Plasmas, C.E.A., B.P. No. 6, 92, Fontenay-aux-Roses (Seine), France
44. Derek Boyd, Department of Physics, University of Maryland, College Park, MD 20742
45. D. Cassel, Department of Physics, Cornell University, Ithaca, NY 14853
46. C. M. Celata, Department of Physics, University of Maryland, College Park, MD 20742
47. Center for Plasma Physics and Thermonuclear Research, University of Texas, Austin, Texas 78712
48. D. Choi, Center for Plasma Physics and Thermonuclear Research, University of Texas, Austin, TX 78712
49. J. F. Clarke, Division of Magnetic Fusion Energy, Department of Energy, Washington, DC 20545
50. T. Consoli, Centre d'Etudes Nucleaires de Grenoble, Avenue des Martyrs, 38, Grenoble, France
51. Controlled Thermonuclear Research Library, Argonne National Laboratory, 9700 S. Cass Avenue, Argonne, IL 60439
52. Controlled Thermonuclear Research Library, Lawrence Livermore Laboratory, P.O. Box 808, Livermore, CA 94550

53. CTR Reading, c/o Jay Borris, Plasma Physics Division, Naval Naval Research Laboratories, Washington, DC 20390

54. CTR Reading Room, Department of Physics and Astronomy, University of Maryland, College Park, MD 20742

55. CTR Reading Room, c/o B. D. Fried, Physics, Department, University of California, Los Angeles, CA 90024

56. CTR Reading Room, c/o Roy Gould, California Institute of Technology, Pasadena, CA 91103

57. CTR Reading Room, c/o R. Gross, Plasma Research Laboratory, Columbia University, New York, NY 10027

58. CTR Reading Room, c/o T. Kammash, 103 Research Administration Building, North Campus, University of Michigan, Ann Arbor, MI 48105

59. CTR Reading Room, c/o D. W. Kerst, Department of Physics, Sterling Hall, Univeristy of Wisconsin, Madison, WI 53706

60. CTR Reading Room, c/o W. B. Thomson, Physics Department, University of California, San Diego, CA 92037

61. A. M. Dupas, Documentation S.I.G.N., Department of de la Physique du Plasma, et de la Fusion Controlée, Association Euratom-CEA, B.P. 85, Grenoble, France

62. H. H. Fleischmann, Department of Applied Physics, Cornell University, Ithaca, NY 14853

63. Gerd Fussman, Max-Planck-Institut für Plasmaphysik, 8046 Garching bei München, Federal Republic of Germany

64. D. Harrill, Department of Physics, Cornell University, Ithaca, NY 14853

65. I. H. Hutchinson, Alcator Group, Francis Bitter National Magnet Laboratory, Massachusetts Institute of Technology, Cambridge, MA 02139

66. H. E. Knoepfel, Laboratorio Gas Ionizzati, C.P. 65, 00044 Frascati (Roma), Italy

67. Librarian, Culham Laboratory, Abingdon, Oxon, OX 14 3DB, England

68. Librarian, Max-Planck-Institut für Plasmaphysik, 8046 Garching bei München, Federal Republic of Germany

69. Library, Centre de Récherches en Physique des Plasmas, 21 Avenue des Bains, 1007 Lausanne, Switzerland

70. Library, FOM-Instituut voor Plasma Fysica, Rijnhuizen, Jutphaas, the Netherlands

71. Library, Laboratorio Gas Ionizzati, C.P. 65, 00044 Frascati (Roma), Italy

72. C. S. Liu, Department of Physics, University of Maryland, College Park, MD 20742

73. S. Mirnov, Kurchatov Institute of Atomic Energy, 46 Ulitsa Kurchatov, P.O. Box 3402, Moscow, U.S.S.R.

74. G. Mischke, Division of Magnetic Fusion Energy, Mail Code G-234, Department of Energy, Washington, DC 20545

75. K. Molvig, Alcator Group, Francis Bitter National Magnet Laboratory, Massachusetts Institute of Technology, Cambridge, MA 02139

76. J. Norem, Controlled Fusion Division, Argonne National Laboratory, 9700 S. Cass Avenue, Argonne, IL 60439

77. T. Ohkawa, General Atomic Co., P.O. Box 81608, San Deigo, CA 92138

78. Plasma Physics Group, Department of Engineering Physics, Australian National University, P.O. Box 4, Canberra, A.C.T. 2600, Australia

79. Plasma Physics Library, Princeton Plasma Physics Laboratory, Princeton University, P.O. Box 451, Princeton, NJ 08540

80. Plasma Physics Reading Room, Room 20A-222, Massachusetts Institute of Technology, Cambridge, MA 02139

81. Q Division Library, c/o F. L. Ribe, Los Alamos Scientific Laboratory, P.O. Box 1663, Los Alamos, NM 87544

82. M. S. Rabinovich, Lebedev Institute of Physics, Academy of Sciences of the U.S.S.R., Leninsky Prospect 53, Moscow, U.S.S.R.

83. Research Information Center, Institute of Plasma Physics, Nagoya University, Nagoya, Japan

84. F. Stauffer, Department of Physics, University of Maryland, College Park, MD 20742

85. J. D. Strachan, Princeton Plasma Physics Laboratory, Princeton University, P.O. Box 451, Princeton, NJ 08540

86. Thermonuclear Laboratory, Kurchatov Institute of Atomic Energy, 46 Ulitsa Kurchatova, P.O. Box 3402, Moscow, U.S.S.R.

87. Thermonuclear Library, Japan Atomic Energy Research Institute, Tokai, Naka, Ibaraki, Japan

88. Versator Group, c/o, G. Bekefi, Department of Physics, Massachusetts Institute of Technology, Cambridge, MA 02139

89. S. von Goeler, Princeton Plasma Physics Laboratory, Princeton University, P.O. Box 451, Princeton, NJ 08540

90. J. Wilkins, Department of Physics, Cornell University, Ithaca, NY 14853

91-99. S. J. Zweben, c/o Department of Physics, University of California, Los Angeles, CA 90024

100. Director, Research and Technical Support Division, DOE-ORO, P.O. Box E, Oak Ridge, TN 37830

101-127. Technical Information Center, P.O. Box 62, Oak Ridge, TN 37830